

Circular geodesics in the field of double-charged dilatonic black holes

Kuantay Boshkayev,^{1,2,3,*} Gulnara Suliyeva,^{1,4,†} Vladimir Ivashchuk,^{5,6,‡} and Ainur Urazalina^{1,2,§}

¹*Al-Farabi Kazakh National University, Al-Farabi av. 71, 050040 Almaty, Kazakhstan.*

²*National Nanotechnology Laboratory of Open Type,
Al-Farabi av. 71, Almaty 050040, Kazakhstan.*

³*International University of Information Technology,
Manas st. 34/1, 050040 Almaty, Kazakhstan.*

⁴*Fesenkov Astrophysical Institute, Observatory 23, 050020 Almaty, Kazakhstan.*

⁵*Center for Gravitation and Fundamental Metrology, VNIIMS,
46 Ozyornaya St., Moscow 119361, Russian Federation.*

⁶*Institute of Gravitation and Cosmology, Peoples' Friendship University of Russia (RUDN University),
6 Miklukho-Maklaya St., Moscow 117198, Russian Federation*

(Dated: June 6, 2023)

A non-extreme dilatonic charged (by two “color electric” charges) black hole solution is considered in a 4-dimensional gravity model including two scalar (dilaton) fields and two Abelian vector fields. Scalar and vector fields interact through exponential terms which contain two dilatonic coupling vectors. The solution is governed by a dimensionless parameter a ($0 < a < 2$), which is a certain function of dilatonic coupling vectors. The paper presents solutions for timelike and null circular geodesics which may play an important role in different astrophysical problems, including quasinormal modes of various test fields in the eikonal approximation. For $a = 1/2, 1, 3/2, 2$ the innermost stable circular orbit (ISCO) radii are presented and analysed.

Keywords: black holes, timelike geodesics, null geodesics, scalar fields, Abelian vector fields, ISCO.

1. INTRODUCTION

After the discovery of gravitational waves in 2016, the interest in the physics of stellar-mass black holes has begun to grow rapidly [1]. Gravitational waves were originally postulated by Einstein over a century ago. Their long search led to the creation of huge super-sensitive laser interferometers LIGO, VIRGO and others, and the development of the latest highly precise methods of detection and data analysis [2].

Observations and studies of the motion of stars at the heart of the Milky Way galaxy have confirmed the existence of a supermassive black hole [3–5]. These surveys provide information about the star clusters near the galactic center and the black hole mass which is used by researchers to test the predictions of general relativity [6].

In addition, the imaging process of the shadow of the supermassive black holes at the center of the M87 galaxy and in the Milky Way galaxy has required remarkable ingenuity and cohesion among scientists around the world [7, 8]. For these purposes, our entire planet was used as one giant radio telescope, consisting of separate groups of telescopes

scattered in all continents. The presence of the image of a black hole shadow and its analysis verify the correctness and reliability of general relativity. All discoveries over the past 60 years testify to the significance and relevance of research in this direction.

At the same time, in addition to general relativity, there are various modified and extended theories of gravity, where alternative black holes with extra parameters exist [9–15]. However, to date, within the range of observational errors, those black holes cannot be for 100% distinguished from ordinary Schwarzschild, Reissner-Nordström, and Kerr black holes [16].

Commonly observational data is used as an important tool for constraining black hole parameters in those theories [17–19]. This fact makes it possible to examine black holes with “colored charges” when there are scalar fields. Classical Schwarzschild and Reissner-Nordström black holes, as well as various models of dilatonic black holes with two colored electric charges are considered here.

The dilaton is a hypothetical scalar field particle. It appears in the metric through the introduction of coupling vectors (constants), which, in turn, define a new particular subclass of black holes. In limiting cases, dilatonic solutions reduce to the Schwarzschild and Reissner-Nordström solutions, depending on the values of the coupling vectors. Since the dilaton has not been discovered yet, it would be interesting to investigate effects associated with its presence.

In this paper we consider the possibility of dis-

*kuantay@mail.ru

†g.suliyeva@mail.ru

‡ivashchuk@mail.ru

§y.a.a.707@mail.ru

tinguishing ordinary astrophysical black holes from dilatonic ones. In this regard, the main objective of the paper is to study the motion of test particles and photons in circular orbits in the gravitational field of astrophysical and dilatonic black holes with different color charges and coupling vectors.

To achieve this goal, the following problems are posed:

- Obtaining geodesic equations in the field of dilatonic black holes using the Lagrange formalism.
- Calculation of the angular momentum, the energy, the effective potential of test particles and photons, and the radii of the innermost stable circular orbits in the field of dilatonic black holes.

The solutions of dilatonic dyonic black holes with an arbitrary coupling constant and a canonical scalar field have been considered in Refs. [20–23]. The solutions were obtained up to the solutions of two master equations for moduli functions. Some physical parameters of the solutions were also obtained: gravitational mass, scalar charge, Hawking temperature, black hole area entropy, and parameterized post-Newtonian (PPN) parameters. While in Ref. [20–22] only the physical characteristics of black holes were studied, in Ref. [23] quasi-normal modes of a massless test scalar field were studied in the background of a gravitational field for a non-extremal dilatonic dyonic black hole.

Timelike and null geodesics, for example circular ones, play an important role in various astrophysical context, including accretion disks, quasiperiodic oscillations, quasinormal modes of various test fields in the eikonal approximation [24] and shadows of supermassive black holes [25, 26]. These results and studies will allow one to distinguish ordinary black holes from dilatonic ones [17].

The novelty of the work resides in the fact that the geodesics of test particles in the gravitational field of dilatonic black holes with two scalar fields and two-color electric charges will be studied for the first time. In the past, some of us have investigated geodesics in the context of standart black holes, naked singularities, and spinning deformed relativistic compact objects [27–30].

In Ref. [31], geodesics around rotating black hole mimickers are studied, given by the exact solution of the stationary and axially symmetric field equations in vacuum, known as the δ -Kerr metric. The authors study its optical properties based on a ray-tracing code for photon motion, characterize the apparent shape of the shadow of a compact object, and compare it with a Kerr black hole. In order to obtain

qualitative estimates related to the observed shadow of a supermassive compact object in the M87 galaxy, the authors are guided by the values of the object's spin a and observation inclination angle close to the measured values. It has been shown that, based on only one set of shadow edge observations, it is not possible to rule out the δ -Kerr solution as a viable source of geometry outside the compact object.

It was shown in [32] that from a geometric point of view it is impossible to distinguish electrically and magnetically charged Reissner-Nordström black holes. One of the ways to describe the differences between these solutions is to study the dynamical motion of charged test particles near a charged black hole and study the effect of charge coupling parameters on the stability of circular orbits. The authors investigate the synchrotron radiation of charged particles accelerated by a charged black hole and estimate the intensity of the relativistic radiation of charged particles.

Recently in Ref. [33] the authors have studied closed photon orbits in spherically-symmetric static solutions of supergravity theories, a Horndeski theory, and a theory of quintessence. These orbits lie in what is called a photon sphere (anti-photon sphere) if the orbit is unstable (stable). It was shown that in all the asymptotically flat solutions examined that admit a regular event horizon, and whose energy-momentum tensor satisfies the strong energy condition, there is one and only one photon sphere outside the event horizon.

Note that while in [34–37] the features of dilatonic black holes are studied, in [31, 32, 38] various solutions to the field equation are considered, which in the limiting case describe ordinary black holes. Refs. [31–33, 38] also study geodesics, which may differ in the field of ordinary black holes. There are some works studying the motion of test particles and photons around static [39–43] and rotating [44, 45] dilatonic black holes in different theories of gravity. To the knowledge of the authors, geodesics around dilatonic black holes with two scalar fields and two vector fields have not been studied elsewhere in the literature.

In this paper, a solution for a charged dilaton black hole (BH) (it is S-dual to dyonic-like solution from [23]) and a particular solutions for null geodesics are considered. It should be noted that there is some interest in spherically symmetric solutions see Refs. [46–49] and references there. These solutions appear in gravitational models with scalar fields and antisymmetric forms. In our analyses, we follow the methodology of [50], where the motion of neutral test particles is studied in the field of a Reissner-Nordström black hole.

The paper is organised as follows: in Section 2 we present charged black solutions with two scalar (dilation) fields and two Abelian vector fields and consider their main characteristics. In Section 3 we examine the geodesics of neutral test particles and photons, derive the expressions for energy, angular momentum, effective etc, study their behavior and analyze the stability of circular geodesics. In Section 4 we summarise our conclusion and discuss perspectives.

2. CHARGED BLACK HOLE SOLUTION

The action of a model containing two scalar fields, 2-form and dilatonic coupling vectors is given by

$$S = \frac{1}{16\pi G} \int d^4x \sqrt{|g|} \left\{ R[g] - g^{\mu\nu} \partial_\mu \vec{\varphi} \partial_\nu \vec{\varphi} - \frac{1}{2} e^{2\vec{\lambda}_1 \vec{\varphi}} F_{\mu\nu}^{(1)} F^{(1)\mu\nu} - \frac{1}{2} e^{2\vec{\lambda}_2 \vec{\varphi}} F_{\mu\nu}^{(2)} F^{(2)\mu\nu} \right\}, \quad (2.1)$$

where $g = g_{\mu\nu}(x) dx^\mu \otimes dx^\nu$ is the metric, $|g| = |\det(g_{\mu\nu})|$, $\vec{\varphi} = (\varphi^1, \varphi^2)$ is the vector of scalar fields belonging to \mathbb{R}^2 , $F^{(i)} = dA^{(i)} = \frac{1}{2} F_{\mu\nu}^{(i)} dx^\mu \wedge dx^\nu$ is the 2-form with $A^{(i)} = A_\mu^{(i)} dx^\mu$, $i = 1, 2$; G is the gravitational constant, $\vec{\lambda}_1 = (\lambda_{1i}) \neq \vec{0}$, $\vec{\lambda}_2 = (\lambda_{2i}) \neq \vec{0}$ are the dilatonic coupling vectors obeying

$$\vec{\lambda}_1 \neq \vec{\lambda}_2, \quad (2.2)$$

and $R[g]$ is the Ricci scalar. Here and in what follows we set $G = c = 1$ (where c is the speed of light in vacuum.)

We consider a so-called double-charged black hole solution to the field equations corresponding to the action (2.1) which is defined on the (oriented) manifold

$$\mathcal{M} = \mathbb{R} \times (2\mu, +\infty) \times S^2, \quad (2.3)$$

and has the following form

$$ds^2 = H^a \left\{ -H^{-2a} \left(1 - \frac{2\mu}{R} \right) dt^2 + \frac{dR^2}{1 - \frac{2\mu}{R}} + R^2 d\Omega^2 \right\}, \quad (2.4)$$

$$\varphi^i = \nu^i \ln H, \quad (2.5)$$

with the 2-form defined by

$$F^{(1)} = \frac{Q_1}{H^2 R^2} dt \wedge dR, \quad F^{(2)} = \frac{Q_2}{H^2 R^2} dt \wedge dR, \quad (2.6)$$

where Q_1 and Q_2 are the (color) electric charges, $\mu > 0$ is the extremality parameter, $d\Omega^2 = d\theta^2 +$

$\sin^2 \theta d\phi^2$ is the canonical metric on the unit sphere S^2 ($0 < \theta < \pi$, $0 < \phi < 2\pi$), $\tau = \sin \theta d\theta \wedge d\phi$ is the standard volume form on S^2 and the moduli function is adopted as

$$H = 1 + \frac{P}{R}, \quad (2.7)$$

with $P > 0$ obeying

$$P(P + 2\mu) = \frac{1}{2} Q^2, \quad (2.8)$$

or equivalently

$$P = -\mu + \sqrt{\mu^2 + \frac{1}{2} Q^2}. \quad (2.9)$$

All the remaining parameters of the solution are defined as follows¹

$$a = \frac{(\vec{\lambda}_1 - \vec{\lambda}_2)^2}{\Delta}, \quad (2.10)$$

$$\Delta \equiv \frac{1}{2} (\vec{\lambda}_1 - \vec{\lambda}_2)^2 + \vec{\lambda}_1^2 \vec{\lambda}_2^2 - (\vec{\lambda}_1 \vec{\lambda}_2)^2, \quad (2.11)$$

$$\nu^i = \frac{\lambda_{1i} \vec{\lambda}_2 (\vec{\lambda}_2 - \vec{\lambda}_1) + \lambda_{2i} \vec{\lambda}_1 (\vec{\lambda}_1 - \vec{\lambda}_2)}{\Delta}, \quad (2.12)$$

$i = 1, 2$ and

$$Q_1^2 = \frac{\vec{\lambda}_2 (\vec{\lambda}_2 - \vec{\lambda}_1)}{2\Delta} Q^2, \quad Q_2^2 = \frac{\vec{\lambda}_1 (\vec{\lambda}_1 - \vec{\lambda}_2)}{2\Delta} Q^2. \quad (2.13)$$

Here the following additional restrictions on dilatonic coupling vectors are imposed

$$\vec{\lambda}_1 (\vec{\lambda}_1 - \vec{\lambda}_2) > 0, \quad \vec{\lambda}_2 (\vec{\lambda}_2 - \vec{\lambda}_1) > 0. \quad (2.14)$$

We note that

$$\Delta > 0, \quad (2.15)$$

is valid for $\vec{\lambda}_1 \neq \vec{\lambda}_2$.

Due to relations (2.14) and (2.15) the Q_s^2 are well-defined. Note that the restrictions (2.14) imply relations $\vec{\lambda}_s \neq \vec{0}$, $s = 1, 2$, and (2.2).

Indeed, in this case we have the sum of two non-negative terms in (2.12): $(\vec{\lambda}_1 - \vec{\lambda}_2)^2 > 0$ and

$$C = \vec{\lambda}_1^2 \vec{\lambda}_2^2 - (\vec{\lambda}_1 \vec{\lambda}_2)^2 \geq 0, \quad (2.16)$$

¹ It should be emphasized that for vanishing $a \rightarrow 0$, $\nu^i \rightarrow 0$, $Q_i \rightarrow 0$ and $\varphi^i \rightarrow 0$ and the line element Eq. (2.4) reduces to the Schwarzschild metric.

due to the Cauchy-Schwarz inequality. Moreover, $C = 0$ if and only if vectors $\vec{\lambda}_1$ and $\vec{\lambda}_2$ are collinear. Relation (2.16) implies

$$0 < a \leq 2. \quad (2.17)$$

For non-collinear vectors $\vec{\lambda}_1$ and $\vec{\lambda}_2$ we get $0 < a < 2$ while $a = 2$ for collinear ones.

This solution may be verified just by a straightforward substitution into the equations of motion.

In addition, in Ref. [23], the definition of gravitational mass was obtained in relation to μ and P parameters:

$$M = \mu + \frac{a}{2}P. \quad (2.18)$$

The following relations can be found/verified from Eqs. (2.10)-(2.13)

$$\vec{v}^2 = \frac{(\vec{\lambda}_1 - \vec{\lambda}_2)^2(\vec{\lambda}_1^2\vec{\lambda}_2^2 - (\vec{\lambda}_1\vec{\lambda}_2)^2)}{\Delta^2} = \frac{a(2-a)}{2}, \quad (2.19)$$

and

$$Q_1^2 + Q_2^2 = \frac{a}{2}Q^2. \quad (2.20)$$

The calculation of scalar curvature for the metric $ds^2 = g_{\mu\nu}dx^\mu dx^\nu$ in (2.4) yields [23]

$$R[g] = \frac{a(2-a)P^2(R-2\mu)}{2R^{4-a}(R+P)^{1+a}}. \quad (2.21)$$

For the Schwarzschild ($a = 0$) and Reissner-Nordström ($a = 2$) solutions one immediately gets $R[g] = 0$.

3. GEODESIC MOTION

Geodesics is a fundamental tool for understanding the motion of test particles in the field of dilatonic black holes, and can provide valuable insights into the nature of these objects and their effects on surrounding spacetime.

Geodesics can be derived from the Lagrangian

$$\mathcal{L} = \frac{1}{2}g_{\alpha\beta}(x)\dot{x}^\alpha\dot{x}^\beta, \quad (3.1)$$

using the Euler-Lagrange equations:

$$\frac{d}{d\tau} \left(\frac{\partial \mathcal{L}}{\partial \dot{x}^\alpha} \right) - \frac{\partial \mathcal{L}}{\partial x^\alpha} = 0, \quad (3.2)$$

where $\dot{x}^\alpha = dx^\alpha/d\tau = u^\alpha$ is the 4-velocity vector, e.g. of a test particle, moving along the curve $x^\alpha(\tau)$, τ is the proper time for massive particles moving

along timelike geodesics and affine parameter in case of null geodesics, respectively, and $\alpha = 0, 1, 2, 3$. The generalized momentum $p_\alpha = g_{\alpha\beta}(x)\dot{x}^\beta$ for Lagrangian (3.1) is normalized as :

$$g^{\alpha\beta}(x)p_\alpha p_\beta = g_{\alpha\beta}(x)u^\alpha u^\beta = -k, \quad (3.3)$$

where $k = -1, 0, 1$ for spacelike, null and timelike geodesics, correspondingly. For general k the quantity $(-k/2)$ is the energy integral of motion for the Lagrangian (3.1). For simplicity we do not consider spacelike geodesics in the paper.

We consider null or timelike geodesics in the equatorial plane ($\theta = \pi/2$). In this case, the Lagrangian for the metric given by Eq. (2.4) reads

$$\mathcal{L} = \frac{1}{2}H^a \left[-H^{-2a} \left(1 - \frac{2\mu}{R} \right) \dot{t}^2 + \frac{\dot{R}^2}{1 - \frac{2\mu}{R}} + R^2 \dot{\phi}^2 \right]. \quad (3.4)$$

For cyclic coordinates t and ϕ one obtains the integrals of motion

$$\tilde{E} = H^{-a} \left(1 - \frac{2\mu}{R} \right) \dot{t}, \quad \tilde{L} = H^a R^2 \dot{\phi}, \quad (3.5)$$

associated for $k = 1$ with the total energy $E = \tilde{E}m$ and angular momentum $L = \tilde{L}m$ of a test (neutral point-like) particle of mass m , which are the constants of motion. In order to find the equation for the R -coordinate for $\dot{R} \neq 0$ one has to use Eq. (3.3), which has the following form for the line element from Eq. (2.4)

$$-H^{-a} \left(1 - \frac{2\mu}{R} \right) \dot{t}^2 + \frac{H^a \dot{R}^2}{1 - \frac{2\mu}{R}} + H^a R^2 \dot{\phi}^2 = -k. \quad (3.6)$$

This relation reduces to the following differential equation by virtue of Eq. (3.5):

$$-\frac{H^a E^2}{m^2 \left(1 - \frac{2\mu}{R} \right)} + \frac{H^a \dot{R}^2}{1 - \frac{2\mu}{R}} + \frac{H^{-a} L^2}{m^2 R^2} = -k. \quad (3.7)$$

Eq. (3.7) can be presented in terms of the effective potential:

$$\dot{R}^2 + V^2 = \frac{E^2}{m^2}, \quad (3.8)$$

which is explicitly given by

$$V = \sqrt{H^{-2a} \left(1 - \frac{2\mu}{R} \right) \left(H^a k + \frac{L^2}{m^2 R^2} \right)}. \quad (3.9)$$

It may be readily verified that the Lagrange equation for the radial coordinate R is equivalent to the following one

$$\ddot{R} + V \frac{\partial V}{\partial R} = 0. \quad (3.10)$$

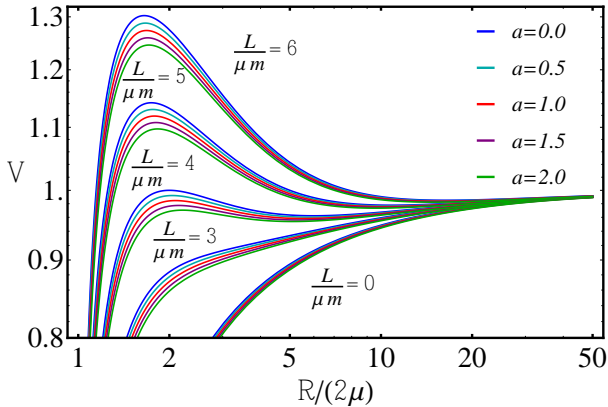


FIG. 1: The effective potential of test particles for $L/(\mu m)=0, 3, 4, 5, 6$ with different $a=0, 0.5, 1, 1.5, 2$ as a function of the dimensionless/normalized radial coordinate $R/(2\mu)$. As one may notice for decreasing L the minimum of the effective potential shifts from right to left.

For $\dot{R} \neq 0$ it can be obtained just by differentiating Eq. (3.8) with respect to parameter τ and then dividing the result by \dot{R} . In case $\dot{R} = 0$ the radial equation reads

$$\frac{\partial V}{\partial R} = 0. \quad (3.11)$$

It does not follow from Eq. (3.8) and should be considered separately.

Now we focus on timelike geodesics ($k = 1$). The behavior of the effective potential as a function of R/μ for the fixed value of $Q/\mu = 0.6$ (which is roughly $P/\mu = 0.0863$) and for different values of $L/(\mu m)$ is illustrated in Fig. 1. The cases of $a = 0$, $a = 1$ and $a = 2$ formally correspond to the Schwarzschild, Sen [51] and Reissner-Nordström solutions, respectively. It is clearly seen that the maximum of the effective potential for $a = 0$ exceeds the maximums for other cases of a .

In Fig. 2 the effective potential at fixed L_{ISCO} is illustrated as a function of the dimensionless radial coordinate $R/(2\mu)$ for different $a=0, 0.5, 1, 1.5, 2$. Dots show the inflection points. As one may see in terms of R and μ these points differ from the standard Schwarzschild and Reissner-Nordström black holes.

Moreover, three dimensional plot of the effective potential with fixed value of $Q/\mu = 0.6$ is shown in Fig. 3 as a function of R/μ and $L/(\mu m)$.

In Table I we present the radii of ISCO, corresponding orbital angular momentum, energy and effective potential of test particles for fixed $Q/\mu = 0.6$

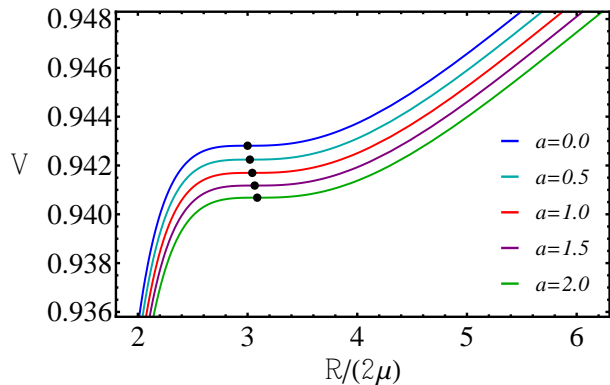


FIG. 2: The effective potential of test particles with L_{ISCO} for different $a=0, 0.5, 1, 1.5, 2$ given in Table I as a function of the dimensionless radial coordinate $R/(2\mu)$. Dots indicate the inflection points ($R_{ISCO}/(2\mu), V_{ISCO} = V(R_{ISCO}/(2\mu))$).

| a | $\frac{R_{ISCO}}{2\mu}$ | $\frac{L_{ISCO}}{\mu m}$ | $\frac{E_{ISCO}}{m}$ | V_{ISCO} |
|-----|-------------------------|--------------------------|----------------------|------------|
| 0.0 | 3.0000 | 3.4641 | 0.9428 | 0.9428 |
| 0.5 | 3.0211 | 3.5176 | 0.9422 | 0.9422 |
| 1.0 | 3.0427 | 3.5716 | 0.9417 | 0.9417 |
| 1.5 | 3.0650 | 3.6260 | 0.9412 | 0.9412 |
| 2.0 | 3.0879 | 3.6809 | 0.9407 | 0.9407 |

TABLE I: Values of parameters $x_{ISCO} = R_{ISCO}/(2\mu)$, $L_{ISCO}/(\mu m)$, E_{ISCO}/m and $V_{ISCO} = V(R_{ISCO}/(2\mu))$ for different a . Note, the net charge here is fixed as $Q/\mu = 0.6$ which is equivalent to $P/\mu = 0.0863$ according to Eq. (2.9). x_{ISCO} has been calculated accounting for Eqs. (3.17)-(3.21).

as a function of parameter a . The graphical representation of these values (points) are shown in Figs. 2-8.

A. Circular geodesics

Here we contemplate circular motions, which are characterized by condition: $\dot{R} = 0$, so $V = E/m$.

The derivative of the effective potential with re-

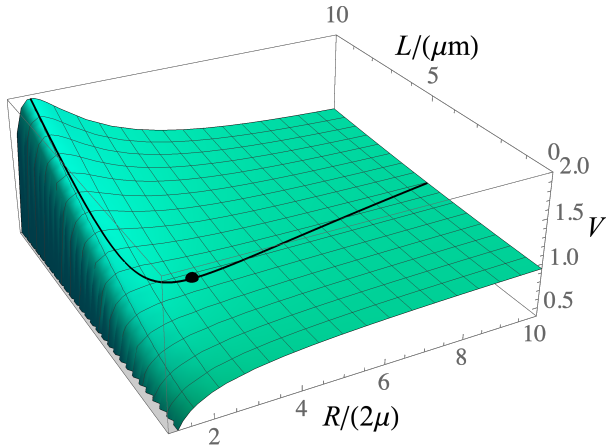


FIG. 3: Three dimensional plot of the effective potential V as a function of $L/(\mu m)$ and R/μ according to Eq. (3.9). The black solid curve indicates V when $L/(\mu m)$ is defined from Eq. (3.13) for circular geodesics. Dot shows the radius of ISCO with corresponding $L/(\mu m)$ and V . Here we only consider the case with $a=1$ and $Q/\mu = 0.6$.

spect to R is given by:

$$\begin{aligned} \frac{\partial V}{\partial R} = & [2R^3 H^{2+a} V]^{-1} \left[H^a (aP(R-2\mu) \right. \\ & + 2\mu(P+R)) + \frac{2L^2}{m^2 R^2} \left\{ R(3\mu-R) \right. \\ & \left. \left. + P(R(a-1) + \mu(3-2a)) \right\} \right]. \end{aligned} \quad (3.12)$$

The radial equation (3.11) implies

$$\frac{L^2}{m^2} = \frac{H^a R^2 [aP(R-2\mu) + 2\mu(P+R)]}{2[R(R-3\mu) + P(R(1-a) + \mu(2a-3))]}, \quad (3.13)$$

which is substituted to Eq. (3.9) to obtain:

$$\frac{E^2}{m^2} = \frac{H^{-a} (R-2\mu)^2 [2R - P(a-2)]}{2R[R(R-3\mu) + P(R(1-a) + \mu(2a-3))]} \quad (3.14)$$

Figs. 4 and 5 show E/m and $L/(\mu m)$ as functions of R/μ for fixed $Q/\mu = 0.6$. Here, the distinctions among all the curves with various a will be larger for larger values of Q/μ .

From Eqs. (3.13) and (3.14), it can be seen, that for timelike geodesics the motion is possible only for for $R(R-3\mu) + P(R(1-a) + \mu(2a-3)) > 0$, with limiting radius:

$$\begin{aligned} R_{\gamma_{\pm}} \equiv & \frac{1}{2} \left[P(a-1) + 3\mu \right. \\ & \left. \pm \sqrt{(P(1-a) - 3\mu)^2 - 4P\mu(2a-3)} \right], \end{aligned} \quad (3.15)$$

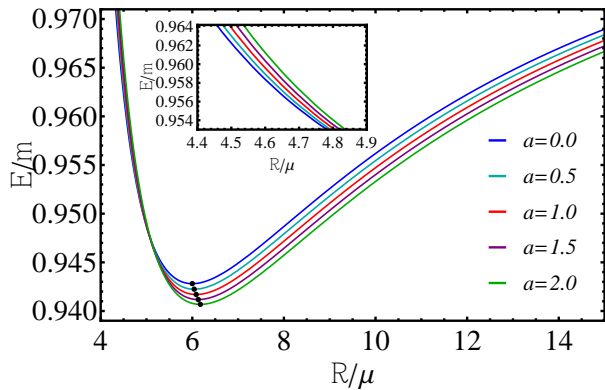


FIG. 4: Energy E/m of test particles as a function of R/μ for cases $a=0.0, 0.5, 1.0, 1.5, 2.0$ when $Q/\mu = 0.6$. Dots indicate R_{ISCO}/μ and corresponding E_{ISCO}/μ see Table I.

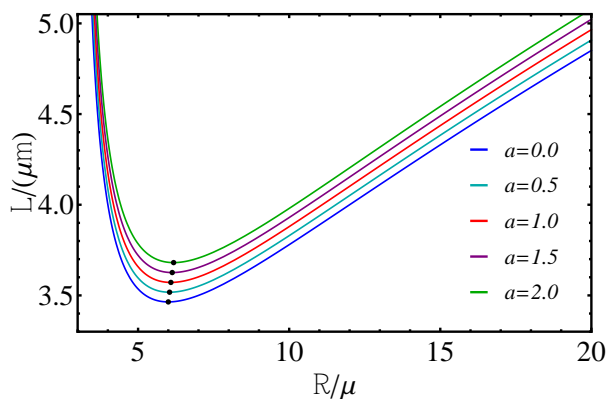


FIG. 5: Orbital angular momentum $L/(\mu m)$ of test particles as a function of R/μ for cases $a=0.0, 0.5, 1.0, 1.5, 2.0$ when $Q/\mu = 0.6$. Dots indicate R_{ISCO}/μ and corresponding $L_{ISCO}/(\mu m)$ see Table I.

where $R_{\gamma_+} = R_0$, in fact, is the radius of the photon sphere and R_{γ_-} is not physical since it is less than 2μ . The dependence of the normalized radius of photon sphere R_0/μ on Q/μ is depicted in Fig. 6. As one can see, the larger Q/μ the larger R_0/μ , at least in this representation of parameters.

B. Innermost stable circular orbits

Innermost stable circular orbit (ISCO) is an important quantity in the study of geodesics in the field of black holes. For example, it plays a crucial role in the physics of accretion disks as it defines the inner radius of the disk. Any massive particle that goes beyond the ISCO will fall onto a black hole,

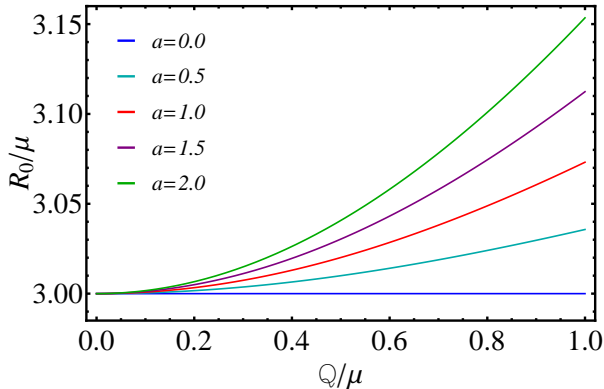


FIG. 6: The location of normalized radii $R_{\gamma+}/\mu = R_0/\mu$ depending on Q/μ .

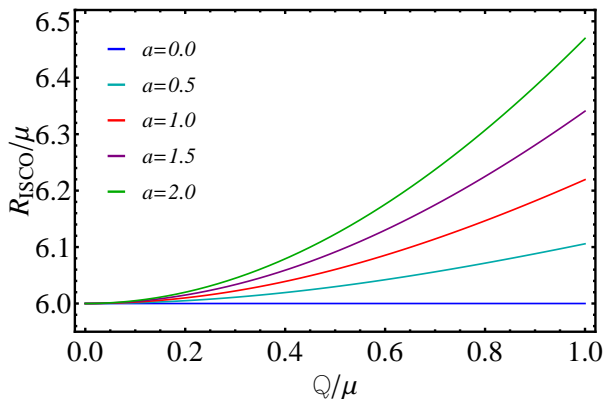


FIG. 7: The location of normalized radii R_{ISCO}/μ as a function of Q/μ .

so the disk is supposed to have a radius larger than the ISCO to maintain its structure. The location of the ISCO, and the properties of the accretion disk (such as its size, temperature, and brightness) can be used to study the features of black holes and their surrounding environment.

Using the condition

$$\frac{\partial^2 V}{\partial R^2} = 0, \quad (3.16)$$

or equivalently by equating to zero the derivatives of Eq. (3.13) or Eq. (3.14) with respect to R one can find R_{ISCO} . For selected values of $a = 0, 0.5, 1, 1.5, 2$ we have the following expressions of R_{ISCO} .

For $a = 0$, which corresponds to the Schwarzschild black hole, the ISCO radius is given by

$$x_{isco}(a = 0) = 3, \quad (3.17)$$

where $x_{isco} = R_{isco}/(2\mu)$.

In Fig. 7 the radii of ISCOs R_{ISCO}/μ are presented versus Q/μ . As one can see, in the represen-

tation for vanishing Q/μ all radii reduce to 6 and for increasing Q/μ , apart from $a=0$ case, R_{ISCO}/μ grows non-linearly.

For $a = 1/2$ the ISCO radius is

$$x_{isco} = \frac{1}{8}(6 - 3p) + \frac{\sqrt{X_{1/2}}}{8(p+2)} + \frac{1}{2} \sqrt{\frac{A_{1/2}}{\sqrt{X_{1/2}}} - \frac{X_{1/2}}{16(p+2)^2}} + T_{1/2}, \quad (3.18)$$

$$X_{1/2} = 16(2+p)^2 Y_{1/2}^{\frac{1}{3}} + (p+2)(72 + 92p + 22p^2 + p^3) + p^2(1+p)(8 + 16p + 7p^2 + p^3) Y_{1/2}^{-\frac{1}{3}},$$

$$Y_{1/2} = \frac{p^3(1+p)\sqrt{R_{1/2}}}{64(p+2)^2} + Z_{1/2},$$

$$R_{1/2} = (2+p)^{-1}(1+p)(2+3p) \left[3968 + 12288p + 12192p^2 + 4392p^3 + 563p^4 + 51p^5 \right],$$

$$Z_{1/2} = 4^{-3}(p+2)^{-3}p^3(1+p)^2 \times \left[128 + 264p + 114p^2 + 10p^3 + p^4 \right],$$

$$A_{1/2} = \frac{1}{8}(432 + 720p + 280p^2 + 9p^4),$$

$$T_{1/2} = \frac{3(72 + 92p + 22p^2 + p^3)}{16(2+p)},$$

where $p = P/2\mu$.

For $a = 1$ which is formally identical to the Sen black hole case, the result is straightforward

$$x_{isco}(a = 1) = 1 + (1+p)^{\frac{1}{3}} + (1+p)^{\frac{2}{3}}. \quad (3.19)$$

For $a = 3/2$ the ISCO radius is

$$x_{isco} = 1 + \frac{p}{2} + X_{3/2}^{\frac{1}{3}} + \frac{Q_{3/2}}{X_{3/2}^{\frac{1}{3}}}, \quad (3.20)$$

$$X_{3/2} = T_{3/2} + \frac{p(1+p)}{16(2+3p)} \sqrt{R_{2/3}},$$

$$T_{3/2} = \frac{32 + 96p + 108p^2 + 51p^3 + 9p^4}{16(2+3p)},$$

$$R_{3/2} = \frac{(2+p) \left[384 + 896p + 544p^2 + 88p^3 - 13p^4 \right]}{2+3p},$$

$$Q_{3/2} = \frac{8 + 20p + 15p^2 + 4p^3}{4(2+3p)}.$$

For $a = 2$, which corresponds to the Reissner-Nordström black hole case, the ISCO radius is

$$x_{isco}(a = 2) = 1 + p + X_2^{\frac{1}{3}} + \frac{1+p+p^2}{X_2^{\frac{1}{3}}}, \quad (3.21)$$

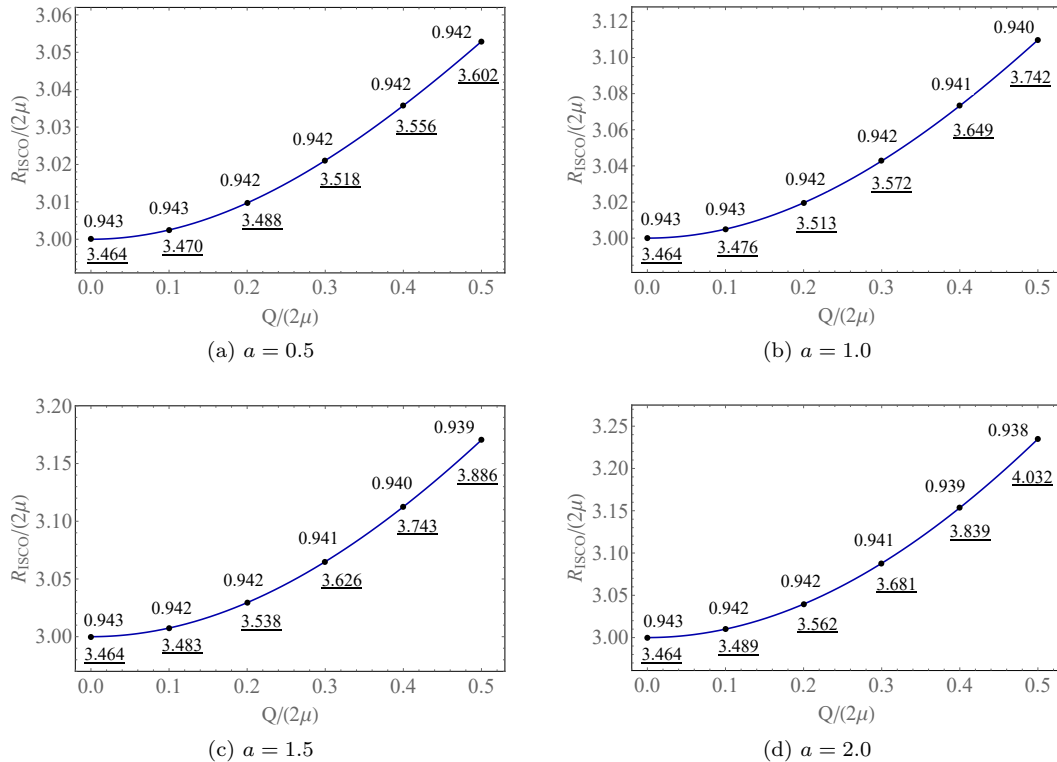


FIG. 8: The normalized by 2μ radius of ISCO as a function of $Q/(2\mu)$ for different $a=0.5, 1, 1.5, 2$. Numbers near the points imply the values of energy E/m and angular momentum $L/(\mu m)$ (underlined numbers) corresponding to a specific ISCO.

where

$$X_2 = \frac{2 + p(1 + p) \left[7 + 4p(1 + p) + \sqrt{5 + 4p(1 + p)} \right]}{2(1 + 2p)}.$$

Using expressions (2.9) and (2.18) allows one to represent Eqs. (3.17) - (3.21) in terms of the gravitational mass M and net charge Q . Correspondingly, in Table II we present μ and P in terms of M and Q depending upon a .

Constraints for Q/M can be obtained from Table II, by requiring $\mu > 0$. Correspondingly, one finds $-2\sqrt{2}/a < Q/M < 2\sqrt{2}/a$ and the case $a = 2$ will give $-\sqrt{2} < Q/M < \sqrt{2}$.

In Ref [23] it was shown that for $a = 2$ case under the radial coordinate transformation, $R = r_{RN} - P$, along with $M_{RN} = \mu + P$, the metric (2.4) coincides with the Reissner-Nordström metric. Taking this into account, one can rewrite Eq. (3.21) in the

following form:

$$\begin{aligned} \frac{r_{isco}^{(RN)}}{M_{RN}} &= 2 + F_{RN}^{1/3} + F_{RN}^{-1/3} \left[4 - \frac{3Q_{RN}^2}{M_{RN}^2} \right], \quad (3.22) \\ F_{RN} &= 8 + \frac{2Q_{RN}^4}{M_{RN}^4} + \frac{Q_{RN}^2}{M_{RN}^2} \left(-9 + \sqrt{G_{RN}} \right), \\ G_{RN} &= 5 - \frac{9Q_{RN}^2}{M_{RN}^2} + \frac{4Q_{RN}^4}{M_{RN}^4}, \end{aligned}$$

which matches with the equation for r_{isco} in Ref. [50]. Here M_{RN} and Q_{RN} are the mass and charge, respectively, of the Reissner-Nordström solution. Besides, the relationship between the charges is given by $Q_{RN}^2 = Q^2/2$, whereas the masses are equal $M_{RN} = M$.

As expected, in the limiting case $Q \rightarrow 0$, R_{ISCO} corresponds to the Schwarzschild value $6M$. In the cases of $0 < a \leq 2$ the values of R_{ISCO} depend upon the ratio of Q/μ . This behaviour is illustrated in Fig. 8. The values of R_{ISCO} at $Q = \mu$ can also be seen in Fig. 7 which are equal to $R_{ISCO}/\mu = 6.10, 6.22, 6.34, 6.46$ for cases $a=0.5, 1.0, 1.5, 2.0$, respectively.

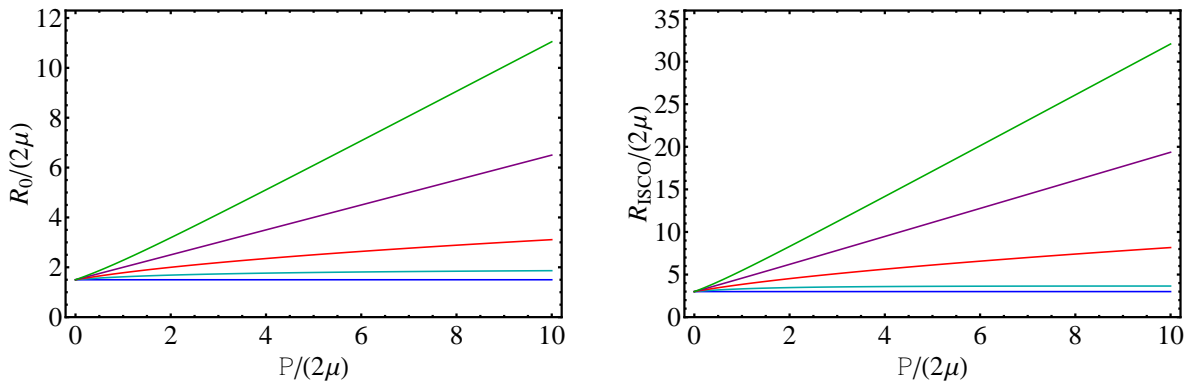


FIG. 9: Left: The normalized by 2μ photon sphere radius as a function of $p = P/(2\mu)$ for different values of a . Right: The radius of ISCOs as a function of $p = P/(2\mu)$ for different values of a .

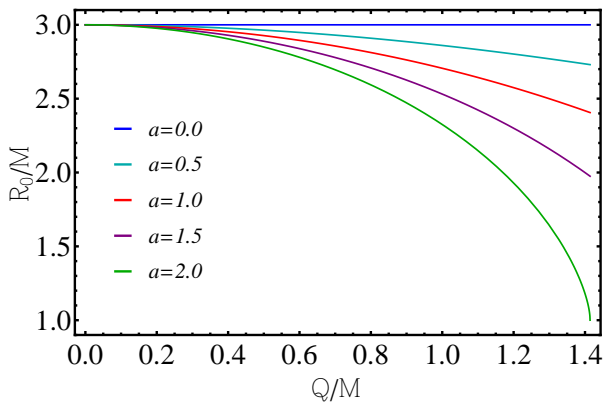


FIG. 10: The location of normalized by gravitational mass M photon sphere radii as a function net charge over gravitational mass Q/M .

The energy and the angular momentum in the last stable circular orbit can be found numerically after plugging expressions (3.18), (3.19), (3.20) and (3.21) into Eqs. (3.13) and (3.14). The results are reported in Table I.

In Fig. 9 the normalized photon sphere radius $R_0/(2\mu)$ (left panel) and $R_{ISCO}/(2\mu)$ (right panel) are given versus $p = P/(2\mu)$. As one can see, also in these representations $R_0/(2\mu)$ and $R_{ISCO}/(2\mu)$ increase with increasing $p = P/(2\mu)$.

In Fig. 10 the normalized by gravitational mass M photon sphere radius is shown versus Q/M for different a . As one may notice, the Schwarzschild case with $a = 0$ possess $R_0/M = 3$ and for other cases $R_0/M < 3$. The Reissner-Nordström case with $a = 2$ has smallest radius $R_0/M = 1$ for the extreme case $Q/M = \sqrt{2}$.

In Fig. 11 (left panel) we present the normalized by gravitational mass M radii of ISCOs as a func-

| a | μ | P |
|-----|---|----------------------------------|
| 0.0 | M | — |
| 0.5 | $\frac{3M}{2} - \frac{1}{4}\sqrt{4M^2 + Q^2}$ | $-2M + \sqrt{4M^2 + Q^2}$ |
| 1.0 | $M - \frac{Q^2}{8M}$ | $\frac{Q^2}{4M}$ |
| 1.5 | $-\frac{M}{2} + \frac{3}{4}\sqrt{4M^2 - Q^2}$ | $2M - \sqrt{4M^2 - Q^2}$ |
| 2.0 | $\sqrt{M^2 - \frac{Q^2}{2}}$ | $M - \sqrt{M^2 - \frac{Q^2}{2}}$ |

TABLE II: Values of parameters μ and P in terms of M and Q depending on a . Note, for vanishing Q one gets $P = 0$ and $\mu = M$. At the same time for vanishing a one recovers the Schwarzschild metric, $\mu = M$ and P disappears in the metric.

tion of net charge over gravitational mass Q/M . As one may see that for increasing charge the radii of ISCOs decrease as one expects in analogy with the Reissner-Nordström solution [50]. In this representation all physical quantities can be measured and used to distinguish charged black holes with different a i.e. different coupling constant vectors $\vec{\lambda}_1$ and $\vec{\lambda}_2$. It is interesting to note, that a similar result was obtained in Fig. 3 (left panel) of Ref. [52] for a neutral test particle in the Sen spacetime. It is shown that for increasing charge over gravitational mass ratio the normalized by gravitational mass M radius r_{ISCO} decreases. In order to compare this result with our findings one should find the relationship between the net charge Q of the present paper

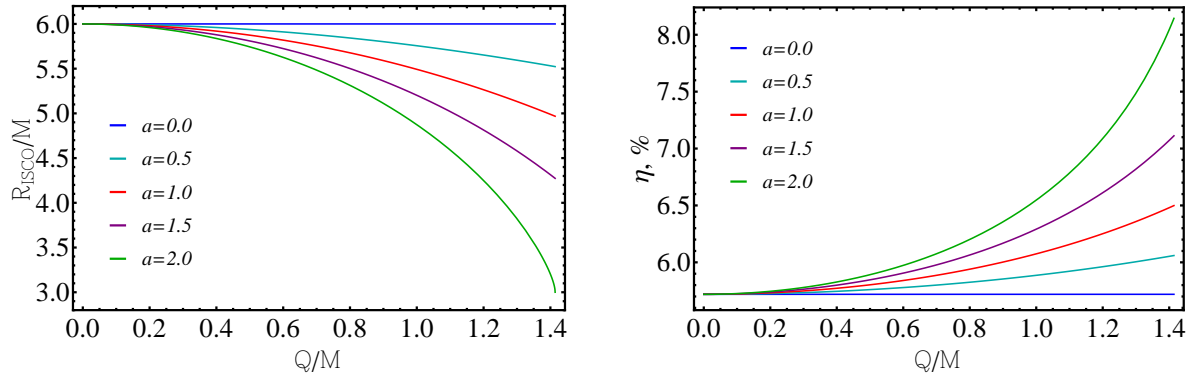


FIG. 11: Left: The normalized by gravitational mass M radii of ISCOs as a function of Q/M for different values of a . Right: The efficiency as a function of Q/M for different values of a .

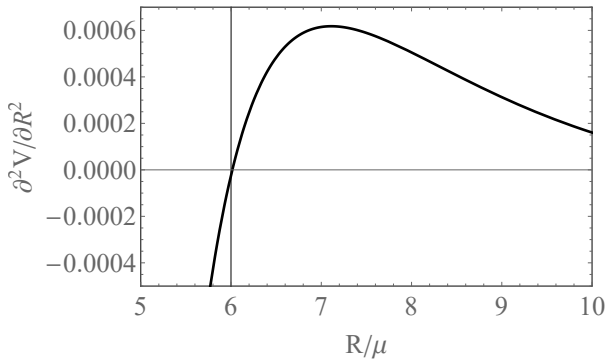


FIG. 12: Representation of the second derivative of the effective potential as a function of R/μ for $a = 0$.

and the one in Ref. [52], which we denote as Q_{Sen} . To do so, one has to give a close look at the line element Eq. (1) in Ref. [52] and compare it with the one considered here when $a = 1$. The two solutions, apart from notations, physical origin and interpretation, are identical. Thus, by comparing the two solutions one finds that $Q = 2Q_{Sen}$ and the value $Q/M = 1.4$ in Fig. 11 left panel for $a = 1$ is equal to $Q_{Sen}/M = 0.7$ in Fig. 3 (left panel) of Ref. [52].

Furthermore, one of the quantities which is of great interest is the efficiency of converting matter into radiation (see for details page 662 of Ref. [53])

$$\eta = [1 - \tilde{E}(R_{ISCO})] \times 100\% \quad (3.23)$$

In Fig. 11 (right panel) the efficiency is shown versus Q/M . As we expected, the efficiency for different values of $a = 0.0, 0.5, 1.0, 1.5, 2.0$ is always larger than the $a = 0$ case.

In general, the circular orbits are allowed in the region $R_0 < R < R_{ISCO}$, however, all those orbits

are unstable. For stability of circular orbits, the following condition must be fulfilled:

$$\frac{\partial^2 V}{\partial R^2} > 0. \quad (3.24)$$

The behavior of the second derivative of the effective potential is depicted in Figs. 12 and 13. From these plots, it can be seen where orbits become stable. The location of ISCO is determined by finding the radius at which the second derivative of the effective potential changes sign from negative to positive.

4. CONCLUSION

In this work we considered the solution for a double-charged dilatonic black hole. We studied circular geodesics of massive neutral test particles and photons for different values of parameters a and P (the latter is directly connected with the net charge Q). We calculated the energy, angular momentum and radius of ISCO of test particles in terms of a , P and μ and investigated in detail their behavior for $a = 0, 1/2, 1, 3/2, 2$ cases, corresponding to various configurations of the double-charged dilatonic black holes.

Our analysis is mainly based on the study of the behavior of an effective potential which defines the position and stability properties of circular orbits. The stability of circular geodesics was analyzed by examining the sign of the second derivative of the effective potential with respect to the radial coordinate. For neutral test particles stable orbits exist only starting from R_{ISCO} up to infinity.

The ISCO radius and photon sphere radius have been calculated for particular values of a . It turned out that, in this representation of the parameters of the line element, for larger a with increasing Q/μ

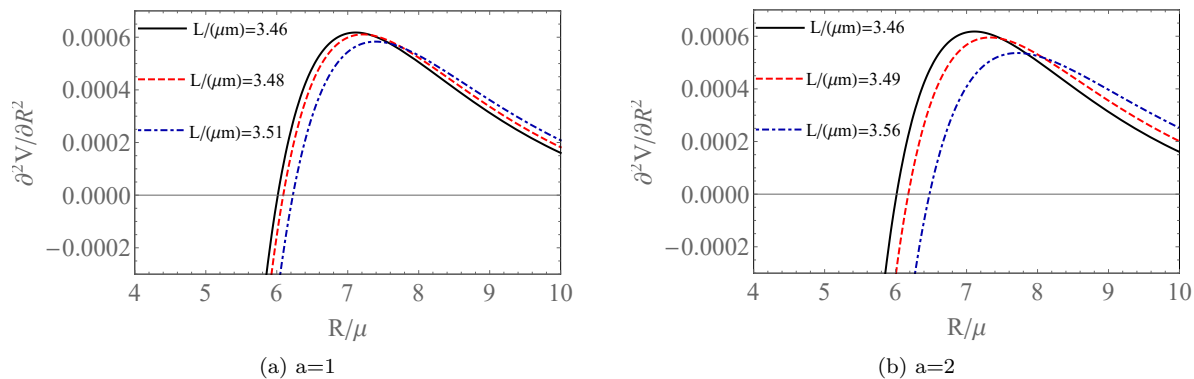


FIG. 13: Second derivative of the effective potential as a function of R/μ . Left: for $a = 1$. Right: for $a = 2$.

In both plots, black, red and blue lines are related to values $Q/\mu = 0, 0.6, 1.0$, respectively. Orbits with $\partial^2 V/\partial R^2 > 0$ are stable, and orbits with $\partial^2 V/\partial R^2 < 0$ are unstable.

the radius of the ISCO and photon sphere radius increase. The photon sphere radius and the ISCO radius have their minimum values $R_0/\mu = 3$ and $R_{ISCO}/\mu = 6$, respectively, in the Schwarzschild limiting case ($a=0$).

However, in the representation of the net charge over gravitational mass the situation is utterly opposite. For the Schwarzschild case ($a = 0$) one gets the largest values for the photon sphere and ISCO radii $3M$ and $6M$, respectively, and for the Reissner-Nordström case ($a = 2$) one obtains M and $3M$, respectively. Taking into consideration Table II for $a = 2$ and $Q/M = \sqrt{2}$ the parameter P will be equal to M . Correspondingly, the photon sphere and ISCO radii will be equal to $2M$ and $4M$, respectively, if one uses the coordinate transformation $r_{RN} = R + P$ and the relation between charges $Q_{RN} = Q/\sqrt{2}$. These results are in agreement with the ones reported in Ref. [50].

The efficiency of converting matter into radiation as expected is larger for the Reissner-Nordström case $\eta = 8.14\%$ and smaller for the Schwarzschild case

$\eta = 5.72\%$ [54]. All other configurations are restricted within these two cases.

This peculiarity can be used to distinguish ordinary or astrophysical black holes from the double-charged dilatonic black holes.

It would be interesting to extend the analyses of the paper in future studies related to the quasinormal modes at final moments of black hole mergers in binaries, quasiperiodic oscillations in the X-ray systems, radiative flux and spectral luminosity of accretion disks around astrophysical black holes.

Acknowledgements

KB thanks professors Daniele Malafarina and Hernando Quevedo for fruitful discussions during the preparation of this paper. KB acknowledges partial support from the Science Committee of the Ministry of Science and Higher Education of the Republic of Kazakhstan (Grant No. AP19680128). For VI the research was funded by RUDN University, scientific project number FSSF-2023-0003.

-
- [1] B. P. Abbott, R. Abbott, T. D. Abbott, M. R. Abernathy, F. Acernese, K. Ackley, C. Adams, T. Adams, P. Addesso, R. X. Adhikari, et al., Phys. Rev. Lett. **116**, 061102 (2016), 1602.03837.
 - [2] B. P. Abbott, R. Abbott, T. D. Abbott, M. R. Abernathy, F. Acernese, K. Ackley, C. Adams, T. Adams, P. Addesso, R. X. Adhikari, et al., Phys. Rev. Lett. **116**, 221101 (2016), 1602.03841.
 - [3] A. M. Ghez, B. L. Klein, M. Morris, and E. E. Becklin, Astrophys. J. **509**, 678 (1998), astro-ph/9807210.
 - [4] A. M. Ghez, M. Morris, E. E. Becklin, A. Tanner, and T. Kremenek, Nature (London) **407**, 349 (2000), astro-ph/0009339.
 - [5] Gravity Collaboration, R. Abuter, A. Amorim, N. Anugu, M. Bauböck, M. Benisty, J. P. Berger, N. Blind, H. Bonnet, W. Brandner, et al., A&A **615**, L15 (2018), 1807.09409.
 - [6] GRAVITY Collaboration, R. Abuter, A. Amorim, M. Bauböck, J. P. Berger, H. Bonnet, W. Brandner, V. Cardoso, Y. Clénet, P. T. de Zeeuw, et al., A&A **636**, L5 (2020), 2004.07187.
 - [7] Event Horizon Telescope Collaboration, K. Akiyama, A. Alberdi, W. Alef, K. Asada,

- R. Azulay, A.-K. Baczko, D. Ball, M. Baloković, J. Barrett, et al., *ApJ Lett.* **875**, L1 (2019), 1906.11238.
- [8] Event Horizon Telescope Collaboration, K. Akiyama, A. Alberdi, W. Alef, J. C. Al-gaba, R. Anantua, K. Asada, R. Azulay, U. Bach, A.-K. Baczko, et al., *ApJ Lett.* **930**, L12 (2022).
- [9] T. P. Sotiriou, *Class. Quant. Grav.* **23**, 5117 (2006), gr-qc/0604028.
- [10] T. Clifton, P. G. Ferreira, A. Padilla, and C. Skordis, *Phys. Rep.* **513**, 1 (2012), 1106.2476.
- [11] A. V. Astashenok, S. Capozziello, and S. D. Odintsov, *JCAP* **01**, 001 (2015), 1408.3856.
- [12] A. V. Astashenok, S. Capozziello, and S. D. Odintsov, *JCAP* **12**, 040 (2013), 1309.1978.
- [13] A. V. Astashenok, S. D. Odintsov, and A. de la Cruz-Dombriz, *Class. Quant. Grav.* **34**, 205008 (2017), 1704.08311.
- [14] S. Capozziello, R. D’Agostino, and O. Luongo, *Int. J. Mod. Phys. D* **28**, 1930016 (2019), 1904.01427.
- [15] A. V. Astashenok, S. Capozziello, S. D. Odintsov, and V. K. Oikonomou, *Phys. Lett. B* **811**, 135910 (2020), 2008.10884.
- [16] Event Horizon Telescope Collaboration, K. Akiyama, A. Alberdi, W. Alef, J. C. Al-gaba, R. Anantua, K. Asada, R. Azulay, U. Bach, A.-K. Baczko, et al., *ApJ Lett.* **930**, L17 (2022).
- [17] P. Pani and V. Cardoso, *Phys. Rev. D* **79**, 084031 (2009), 0902.1569.
- [18] S. Shankaranarayanan and J. P. Johnson, *General Relativity and Gravitation* **54**, 44 (2022), 2204.06533.
- [19] G. Antoniou, A. Papageorgiou, and P. Kanti, *Universe* **9**, 147 (2023), 2210.17533.
- [20] M. E. Abishev, K. A. Boshkayev, V. D. Dzhunushaliev, and V. D. Ivashchuk, *Classical and Quantum Gravity* **32**, 165010 (2015), 1504.07657.
- [21] M. E. Abishev, K. A. Boshkayev, and V. D. Ivashchuk, *European Physical Journal C* **77**, 180 (2017), 1701.02029.
- [22] F. B. Belissarova, K. A. Boshkayev, V. D. Ivashchuk, and A. N. Malybayev, in *Journal of Physics Conference Series* (2020), vol. 1690, p. 012143.
- [23] A. N. Malybayev, K. A. Boshkayev, and V. D. Ivashchuk, *European Physical Journal C* **81**, 475 (2021), 2103.10920.
- [24] R. A. Konoplya, A. F. Zinhailo, and Z. Stuchlík, *Phys. Rev. D* **99**, 124042 (2019), 1903.03483.
- [25] A. Uniyal, R. C. Pantig, and A. Övgün, *Physics of the Dark Universe* **40**, 101178 (2023), 2205.11072.
- [26] G. Lambiase, R. C. Pantig, D. Jyoti Gogoi, and A. Övgün, arXiv e-prints arXiv:2304.00183 (2023), 2304.00183.
- [27] K. Boshkayev, T. Konysbayev, E. Kurmanov, O. Luongo, D. Malafarina, and H. Quevedo, *Phys. Rev. D* **104**, 084009 (2021), 2106.04932.
- [28] K. Boshkayev, E. Gasperín, A. C. Gutiérrez-Piñeres, H. Quevedo, and S. Toktarbay, *Phys. Rev. D* **93**, 024024 (2016), 1509.03827.
- [29] D. Bini, K. Boshkayev, R. Ruffini, and I. Siutsou, *Nuovo Cimento C Geophysics Space Physics C* **36**, 31 (2013), 1306.4792.
- [30] K. A. Boshkayev, H. Quevedo, M. S. Abutalip, Z. A. Kalymova, and S. S. Suleymanova, *International Journal of Modern Physics A* **31**, 1641006 (2016), 1510.02016.
- [31] S. Li, T. Mirzaev, A. A. Abdurjabbarov, D. Malafarina, B. Ahmedov, and W.-B. Han, *Phys. Rev. D* **106**, 084041 (2022), 2207.10933.
- [32] B. Turimov, M. Boboqambarova, B. Ahmedov, and Z. Stuchlík, *European Physical Journal Plus* **137**, 222 (2022).
- [33] M. Cvetič, G. W. Gibbons, and C. N. Pope, *Phys. Rev. D* **94**, 106005 (2016), 1608.02202.
- [34] Y. Huang and H. Zhang, *Phys. Rev. D* **105**, 124056 (2022), 2206.05645.
- [35] Y. Huang and H. Zhang, *European Physical Journal C* **80**, 654 (2020), 2006.01388.
- [36] M. Cadoni, G. D’Appollonio, and P. Pani, *Journal of High Energy Physics* **2010**, 100 (2010), 0912.3520.
- [37] C. Chen, *Progress of Theoretical Physics Supplement* **172**, 161 (2008), 0801.0032.
- [38] F. Sarikulov, F. Atamurotov, A. Abdurjabbarov, and B. Ahmedov, *European Physical Journal C* **82**, 771 (2022).
- [39] Y. Zeng, J.-L. Lü, and Y.-J. Wang, *Chinese Physics Letters* **23**, 1648 (2006).
- [40] C. Blaga, *Serbian Astronomical Journal* **190**, 41 (2015), 1407.1504.
- [41] S. Sarkar, F. Rahaman, I. Radinschi, T. Grammenos, and J. Chakraborty, *Advances in High Energy Physics* **2018**, 5427158 (2018), 1805.00295.
- [42] C. Blaga, P. Blaga, and T. Harko, *Symmetry* **15**, 329 (2023), 2301.07678.
- [43] M. Heydari-Fard, M. Heydari-Fard, and H. R. Sepangi, *Phys. Rev. D* **105**, 124009 (2022), 2110.02713.
- [44] S. Soroushfar, R. Saffari, and E. Sahami, *Phys. Rev. D* **94**, 024010 (2016), 1601.03143.
- [45] K. Flathmann and S. Grunau, *Phys. Rev. D* **92**, 104027 (2015), 1509.03135.
- [46] K. A. Bronnikov and G. N. Shikin, *Soviet Physics Journal* **20**, 1138 (1977).
- [47] G. W. Gibbons and K.-I. Maeda, *Nuclear Physics B* **298**, 741 (1988).
- [48] D. Garfinkle, G. T. Horowitz, and A. Strominger, *Phys. Rev. D* **43**, 3140 (1991).
- [49] D. Garfinkle, G. T. Horowitz, and A. Strominger, *Phys. Rev. D* **45**, 3888 (1992).
- [50] D. Pugliese, H. Quevedo, and R. Ruffini, *Phys. Rev. D* **83**, 024021 (2011), 1012.5411.
- [51] A. Sen, *Phys. Rev. Lett.* **69**, 1006 (1992), hep-th/9204046.
- [52] B. Narzilloev, J. Rayimbaev, S. Shaymatov, A. Abdurjabbarov, B. Ahmedov, and C. Bambi, *Phys. Rev. D* **102**, 044013 (2020), 2007.12462.
- [53] C. W. Misner, K. S. Thorne, and J. A. Wheeler, *Gravitation* (W. H. Freeman and Company, 1973).
- [54] A. H. Bokhari, J. Rayimbaev, and B. Ahmedov, *Phys. Rev. D* **102**, 124078 (2020).